ORIGINAL CONTRIBUTION

Rhinology, 48, 394-400, 2010

Aerodynamic effects of inferior turbinate surgery on nasal airflow - a computational fluid dynamics model*

X.B. Chen[1], S.C. Leong[2], H.P. Lee[1], V.F.H. Chong[3], D.Y. Wang[4]

[1] Department of Mechanical Engineering, National University of Singapore, Singapore
[2] Common Cold Centre and Healthcare Clinical Trials, Cardiff School of Biosciences, Cardiff University, Wales, United Kingdom
[3] Department of Diagnostic Radiology, Yong Loo Lin School of Medicine, National University of Singapore, Singapore
[4] Department of Otolaryngology, Yong Loo Lin School of Medicine, National University of Singapore, Singapore

SUMMARY

Background: *Turbinate reduction surgery may be indicated for inferior turbinate enlargement when conservative treatment fails. The aim of this study was to evaluate the effects of inferior turbinate surgery on nasal aerodynamics using computational fluid dynamics (CFD) simulations.*

Methods: *CFD simulations were performed for the normal nose, enlarged inferior turbinate and following three surgical procedures: 1) resection of the lower third free edge of the inferior turbinate, 2) excision of the head of the inferior turbinate and 3) radical inferior turbinate resection. The models were constructed from MRI scans of a healthy human subject and a turbulent flow model was used for the numerical simulation. The consequences of the three turbinate surgeries were compared with an originally healthy nasal model as well as one with severe nasal obstruction.*

Results: *In the normal nose, the bulk of streamlines traversed the common meatus adjacent to the inferior and middle turbinate in a relatively vortex free flow. When the inferior turbinate was enlarged, the streamlines were directed superiorly at higher velocity and increased wall shear stress in the nasopharynx. Of the three surgical techniques simulated, wall shear stress and intranasal pressures achieved near-normal levels after resection of the lower third. In addition, airflow streamlines and turbulence improved although it did not return to normal conditions. Radical turbinate resection resulted in intra-nasal aerodynamics of atrophic rhinitis.*

Conclusion: *There is little evidence that inspired air is appropriately conditioned following radical turbinate surgery. Partial reduction of the hypertrophic turbinate results in improved nasal aerodynamics, which was most evident following resection of the lower third. The results were based on a single individual and cannot be generalised without similar studies in other subjects.*

Key words: inferior turbinate surgery, airflow pattern, nasal cavity, computational fluid mechanics, turbulence

INTRODUCTION

Nasal obstruction caused by enlarged inferior turbinates is a common presentation in clinical practice. Turbinate reduction surgery may be indicated when conservative treatments such as corticosteroids and antihistamines fail. Reducing the bulkiness of the inferior turbinates will evidently result in improved nasal airflow. However, nasal aerodynamics is far more complex than merely restoring the quantity of air traversing the nasal passages. The evidence base supporting the efficacy of surgical management of the hypertrophic inferior turbinate remains low despite many decades of experience. In a systematic review of the literature, Batra et al. [(1)] reported that there was a paucity of good quality clinical trials evaluating and comparing between the different surgical techniques for inferior turbinate hypertrophy. Few studies utilized objective measures of nasal airflow such as acoustic rhinometry, rhinomanometry, and rhinoresistometry rendering meta-analysis of surgical outcomes impossible. The current gold standard method to objectively assess nasal airflow is rhinomanometry [(2)]. However, this is not routinely utilised in clinical practice and remains predominantly in rhinology research laboratories.

*Received for publication: November 26, 2009; accepted: January 3, 2010

DOI:10.4193/Rhino09.196

Computational fluid dynamics (CFD) is one of the branches of fluid mechanics that uses numerical methods and algorithms to analyze problems, which involve fluid flow. Computers are used to perform the calculations required to simulate the interaction of liquids and gases with surfaces defined by boundary conditions. A small but growing number of rhinology research centres have adapted CFD technology to study nasal airflow, physiology and to simulate outcomes following surgical intervention [3]. CFD offers a highly graphical model to better understand the nature of nasal airflow. This has not been previously possible with other techniques such as rhinomanometry or Mink box simulations. Previous CFD studies have evaluated the effects of septal deviation [4], septal perforation [5,6] and radical sinus surgery [7] on nasal airflow. Studies modelling the effects of turbinate surgery have been published but these were based on the normal healthy nose instead of using a hypertrophic inferior turbinate model [8,9].

The aim of this study was to evaluate the effects of inferior turbinate surgery on nasal aerodynamics using CFD simulations. The airflow changes following three different surgical interventions on the hypertrophic inferior turbinate were studied, and the results compared with airflow of the normal healthy nasal cavity. The intention was to evaluate the outcome of different surgical procedures on a hypertrophic turbinate model and to benchmark the results against the flow pattern of a healthy human subject.

MATERIALS AND METHODS

Overal

Institutional Review Board approval was obtained for this study. Image acquisition, three-dimensional reconstruction, mesh grid formation and computational simulation follows established standard operating procedures of the institution, which have been published previously [4,10], although a summary of the technique is given below.

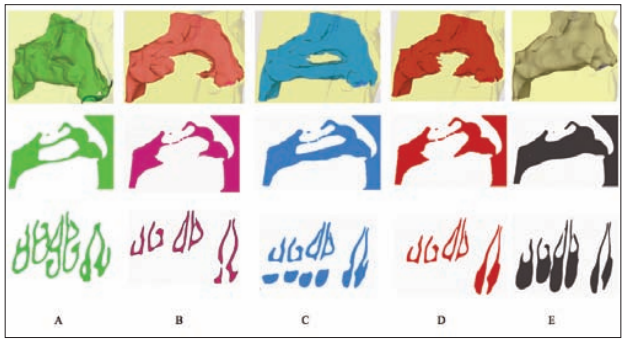

Figure 1. Comparison of the geometry of the nasal cavity. (A) Normal healthy nose. (B) Enlarged inferior turbinate causing nasal obstruction. (C) Lower third of the inferior turbinate excised. (D) Head of the inferior turbinate excised (E) Radical inferior turbinate resection. The figures in the top row represent the three-dimensional image of the respective nasal cavities. Figures in the middle row are the geometrical representation of the nasal cavity in sagittal section. Figures in the bottom row represent the view of the nasal cavity at the corresponding coronal section.

MRI scan

A representative nasal model was obtained from magnetic resonance imaging (MRI) scan of a normal, healthy volunteer (Chinese adult male, 183 cm height and 80 kg mass) without any sino-nasal complaints. Normal and healthy internal nasal cavity was confirmed with endoscopy and acoustic rhinometry. The MRI scans were taken at 1.5 mm intervals and a three-dimensional image was reconstructed using several commercially available softwares such as MIMICS 12.1 (The Materilize Group, Leuven, Belgium), Hypermesh 9.0 (Altair Engineering, Bangalore, India), and TGrid 4.0 (ANSYS, Inc., Canonsburg, PA, USA). Smoothing of the highly corrugated surfaces due to digitization was performed to facilitate computational meshing of the three-dimensional model (Figure 1A). Smoothing of the boundary surface in such relatively larger 3-D nasal cavity will not affect the main flow pattern inside, but will help to decrease computational effort and increase computational efficiency.

The inferior turbinate was then expanded circumferentially by 2 mm to simulate severe obstruction, which corresponded to a two-thirds reduction in the minimum cross-sectional area described in our previous study (Figure 1B) [10]. Surgical techniques simulated included partial (Figures 1C and 1D) and radical inferior turbinate resection (Figure 1E). Two variations of partial resection were simulated: 1) resection of the lower one-third free edge of the turbinate (Figure 1C) and 2) excision of the head of the turbinate in a wedge tapering inferiorly (Figure 1D).

Computational fluid dynamic simulations

Computational fluid dynamic simulations were performed using Fluent 6.3 (ANSYS, Inc.) for the normal nose, severely obstructed nose and the three surgical techniques described above. For

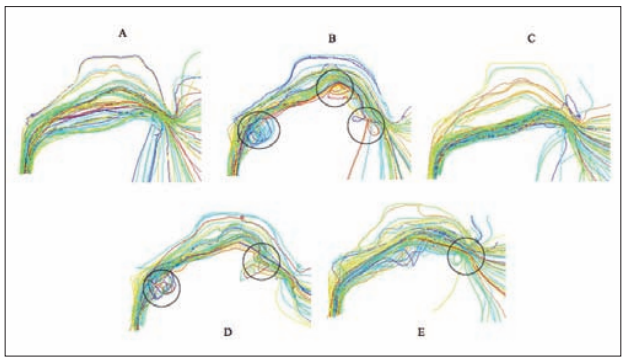

Figure 2. Comparison of the velocity streamlines in the nasal cavity with an inspiratory airflow rate of 17.4 L/min. The vortex areas are circled. (A) Healthy nasal cavity. (B) Enlarged inferior turbinates causing nasal obstruction. (C) Lower third of the inferior turbinate excised. (D) Head of the inferior turbinate excised. (E) Radical inferior turbinate resection.

the CFD simulations, the flow was assumed to be incompressible and quasi-steady. To account for the possible existences of turbulence, the Reynolds (Re) averaged Navier-Stokes equations were solved for the turbulence flow with κ - ω model. The κ - ω model approximation is sufficient to depict the low levels of swirling in the nasal cavity and its ability to predict pressure drop, velocity and shear stress distributions [11,12]. The shear stress transport (SST) option with transitional flow treatment was implemented to capture such complex laminar-transitional-turbulent flow within the nose. The SST model blends between the κ - ω (applied near wall) and κ - ε turbulent model (applied at the main flow domain), which is ideal for flow in the complex geometry of the nasal cavity. The turbulence intensity was set at 6% and the dissipation rate was set at a dissipation length scale of 0.14 cm at the inlet and outlet boundaries. A constant flow rate of 17.4, 34.8 and 52.2 L/min at the nasopharynx area was applied as the boundary condition to simulate calm breathing and quick sniffing conditions. This experimental setting was used given that inspiratory flow rate for a healthy adult can range from 5 L/min to 12 L/min for calm breathing. An extreme flow rate, such as during extreme exertion, may be as high as 150 L/min [13]. At the external enclosure of the face, the pressure inlet boundary condition was applied with gauge pressure equal to zero (atmospheric pressure). The existence of this extra volume (2,040 cm^3) in front of the nose entry would ensure that the entry of gas was in contact with uniform atmosphere gas and would further isolate the artificial boundary condition effects on the simulation results within nasal cavity.

Result analysis

The results of this study were expressed in several ways: 1) streamlines of nasal airflow, 2) nasal resistance, 3) maximum transient velocity, 4) pressure contours, 5) local Reynolds number, 6) wall shear stress distribution and its maximum value, 7) total pressure loss from nostril to nasopharynx. Nasal resistance ($R = \Delta p/Q$), the ratio between pressure change from nostril to nasopharynx and total flow rate, was used to evaluate nasal obstruction, with the units of Pa s/cm3. Local maximum transient velocity was the maximum value observed during the turbulent nasal airflow simulation at the nasal valve region. The local Reynolds number (Re) is a dimensionless number that gives a measure of the ratio between local inertial forces and viscous forces. It quantifies the relative importance of these two types of forces for given flow conditions. The local Reynolds number can be used to characterise different flow regimes, such as laminar or turbulent flow. Laminar flow occurs at relatively lower local Reynolds numbers, where viscous forces are more dominant and flow is characterised by smooth, constant fluid motion. Conversely, turbulent flow occurs at relatively higher local Reynolds numbers and is dominated by inertial forces, which tend to produce random vortices and chaotic flow fluctuations.

RESULTS

Plots of the streamlines for the five simulations of different turbinate conditions showed differences in the presence of vortices in the flows (Figure 2). In the normal nose, most streamlines traversed the common meatus adjacent to the inferior and middle turbinate in a relatively vortex free flow (Figure 2A). In the healthy model, the maximum transient velocity at the nasal valve region was 3.17 m/s. When the inferior turbinate was artificially enlarged to simulate severe obstruction, the streamlines were directed superiorly with vortices occurring at the nasal valve region, olfactory groove and nasopharynx (Figure 2B). The maximum transient velocity increased to 5.59 m/s. The streamlines were predominantly directed along the floor of the nasal cavity and lower part of the common meatus when the lower third of the inferior turbinate was excised (Figure 2C), with a maximum transient velocity of 2.50 m/s and fewer streamlines flowed in the superior part of the nasal cavity as compared to the healthy nose. The vortices in the nasopharynx and nasal valve region persisted, although the vortex in the olfactory groove disappeared following excision of the head of the inferior turbinate (Figure 2D). The maximum transient velocity remained higher than normal at 4.96 m/s. Although fewer vortices occurred after radical turbinectomy (Figure 2E), the streamlines appeared less organised compared to the normal nose. The disorganized streamlines were concentrated on the lower part of the nasal cavity. The maximum transient velocity was lower than normal at 2.69 m/s.

The nasal resistance of this normal healthy nose was 0.032 Pa s/cm^3 at an inspiratory flow rate of 17.4 L/min. The resistance increased to 0.112 Pa s/cm^3 and 0.115 Pa s/cm^3 in the severely obstructed nose and following excision of the head of the inferior turbinate respectively. Excision of the lower third of the turbinate and radical turbinectomy lowered the nasal resistance, 0.025 Pa s/cm^3 and 0.026 Pa s/cm^3, respectively, which was lower than the observed normal value.

In the healthy nose, the pressure contours decreased smoothly along the length of the nasal cavity from nostril to nasopharynx (Figure 3A). A greater pressure gradient was observed anterior to the head of the inferior turbinate, within the nasal valve region. The total pressure difference from the nostril to nasopharynx was 9.28 Pa in healthy nose. The pressure difference was 32.48 Pa in the severely obstructed nose (Figure 3B), which decreased to 7.30 Pa when the lower one-third of the inferior turbinate was excised (Figure 3C). The distribution of pressure contours approximated conditions observed in the normal nose although the magnitude of pressure drop was smaller. The pressure difference increased slightly compared to the severely obstructed nose to 33.38 Pa after resection of the head of the inferior turbinate. As expected, as there was less resistance to nasal airflow after radical turbinectomy, the observed pressure difference fell below normal to 7.71 Pa

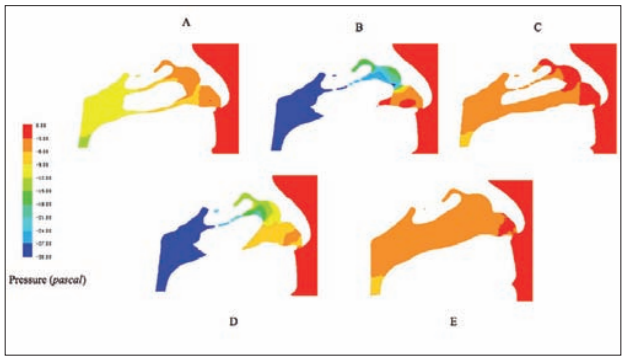

Figure 3. Sagittal cross-section of contour pressure (Pa) at an inspiratory flow rate of 17.4 L/min. (A) Healthy nasal cavity. (B) Enlarged inferior turbinates causing nasal obstruction. (C) Lower third of the inferior turbinate excised. (D) Head of the inferior turbinate excised. (E) Radical inferior turbinate resection.

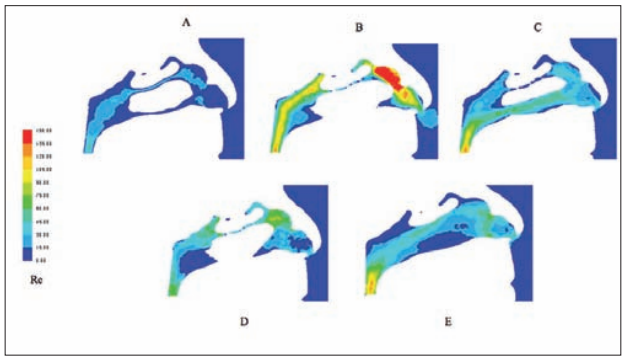

Figure 4. Comparison of local Reynolds (Re) numbers at an inspiratory flow rate of 17.4 L/min. (A) Healthy nasal cavity. (B) Enlarged inferior turbinates causing nasal obstruction. (C) Lower third of the inferior turbinate excised. (D) Head of the inferior turbinate excised. (E) Radical inferior turbinate resection.

(Figure 3E). The contour pressure distribution remained uniform throughout the entire nasal cavity.

The local Reynolds number profiles (Figure 4) correlated with the streamline profiles of the five simulations (Figure 2). Airflow within the normal healthy nasal cavity was relatively laminar as indicated by the smaller Reynolds number distribution. However, airflow was prone to be turbulent (larger Reynolds number distribution) when the nasal cavity became narrower because of inferior turbinate hypertrophy (Figure 4B). The local Reynolds profile appeared to decrease and distribute more smoothly with surgical intervention, although turbinate surgery did not approximate the distribution profile of the normal healthy nose. Of note, the local Reynolds number remained high in the nasopharynx indicating that airflow is relatively more turbulent despite turbinate surgery.

The absolute Reynolds number at the head of the healthy inferior turbinate was 3.45, increasing substantially to 67.5 in the hypertrophic turbinate. Although the Reynolds number reduced with surgical intervention (e.g. 29.7, 46.2 and 27.5 in the cases of lower third, head and radical inferior turbinate resections, respectively), it remained significantly above normal indicating that the area of the resected head in inferior turbinate experienced turbulent airflow.

In the healthy nose, the wall shear stress was generally low to moderate with the maximum stress level at the head of the inferior turbinate of 0.52 Pa (Figure 5A). This area of high stress increased to a maximum of 0.89 Pa when the inferior turbinate was enlarged. The area of high wall shear stress also extended superiorly toward the middle turbinate (Figure 5B). Excision of the lower third of the inferior turbinate appeared to return the wall shear stress profile to near normal distribu-

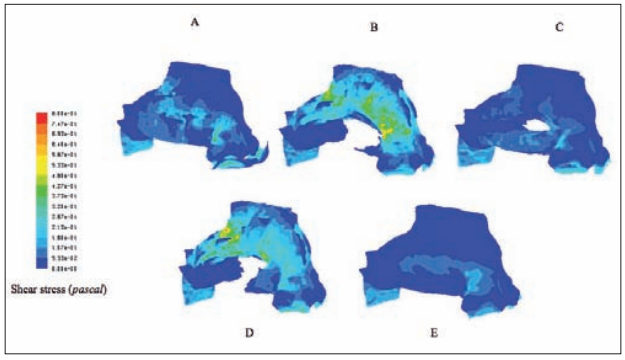

Figure 5. Wall shear stress (Pa) distribution at an inspiratory flow rate of 17.4 L/min. (A) Healthy nasal cavity. (B) Enlarged inferior turbinates causing nasal obstruction. (C) Lower third of the inferior turbinate excised. (D) Head of the inferior turbinate excised. (E) Radical inferior turbinate resection.

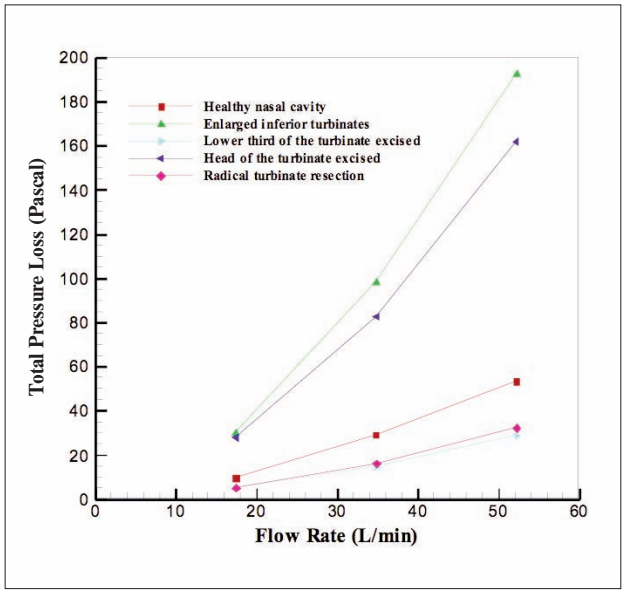

Figure 6. Comparison of total pressure loss with different flow rates.

tion with a maximum wall shear stress of 0.45 Pa, although the larger inferior meatus area was now subjected to increased wall shear stress levels (Figure 5C). Excision of the head of the turbinate merely redirected the airflow posteriorly with increasing high wall shear stress in the nasopharynx (Figure 5D). The maximum wall shear stress doubled to 1.12 Pa compared to normal. When radical turbinectomy was performed, the maximum wall shear stress falls below normal to 0.30 Pa. The distribution of wall shear stress was relatively lower than the normal throughout the nasal cavity.

When the inspiratory flow rate through the nasal cavity was increased for all the five cases, the total pressure loss from the nostril to nasopharynx became greater (Figure 6). This characteristic was most obviously apparent for inferior turbinate hypertrophy and the trend only improved marginally after excision of the head of the turbinate. There was noticeable improvement in the relationship between flow rate and total pressure loss after excision of the lower third of the turbinate and radical turbinate resection.

DISCUSSION

This study has evaluated the effects of partial and total turbinate reduction surgery on the nasal airflow using CFD simulations. Unlike previous simulations, which were performed on healthy models, a hypertrophic inferior turbinate model was used in the present study. We believe the results realistically replicate the aerodynamic changes of patients seeking treatment for nasal obstruction due to inferior turbinate hypertrophy. The results presented are of clinical relevance given that little is known about nasal airflow following turbinate surgery and how changes in post-operative aerodynamics may contribute to complications such as atrophic rhinitis, persistent nasal obstruction and hyposmia.

Conservative turbinate reduction surgery by resecting the lower one-third appeared to result in near-normal Reynolds number profile distribution and wall sheer stress levels. Given that these variables relate to the degree of air-mucosa contact, which is important for air conditioning, the results further support the need to preserve the inferior turbinate whatever surgical technique is used in actual clinical practice. Radical turbinate resection significantly alters nasal airflow resulting in abnormal aerodynamics. The airflow patterns and cross-sectional pressures obtained following radical turbinate resection were comparable to a previously published CFD study on a patient suffering with debilitating atrophic rhinitis [14]. The airstreams within the atrophic nasal cavity were disorganised and turbulent resulting in minimal contact with the remaining nasal mucosa along the septum and lateral wall.

Our simulations corroborated with results reported by Lindemann et al. [8] who modelled air temperature distribution in the healthy nasal cavity following radical turbinate resection. The centre of the airstreams remained cool throughout the nasal cavity and although heat exchange occurred between the areas adjacent to mucosa, the overall warming of inspired air was significantly less than that of the normal healthy nose. As a consequence, the desiccating effect of the abnormal airflow causes crusting and fetor, which are commonly encountered in atrophic rhinitis [15]. Furthermore, the poorly conditioned inspired air may have an adverse effect on the lungs, especially in extreme cold or hot temperature environments [16].

Studies published by Grützenmacher et al. [17,18] using acrylic polymer models of anatomically exact nasal cavities in Mink box experiments, also reported that flow was predominantly in the common meatus in the healthy model. They further reported that nasal airflow became more turbulent and had "unfavourable flow course" following radical excision of the turbinate. Other simulations such as lateral wall hyperplasia and turbinoplasty corroborated with our present simulations. Although the technique used these earlier studies differed significantly to CFD simulations, there was good correlation between the results derived from this two disparate technology.

The importance of the inferior turbinates in air conditioning was described in a detailed study by Hörschler et al. [19] Using CFD simulations on anatomically accurate nasal models, they reported that air conditioning was more closely related to nasal geometry during inspiration than expiration. The relationship of the inferior turbinate within the nasal valve region was important to ensure a homogeneous air velocity distribution and laminar flow throughout the nasal cavity. Furthermore, the large surface area of the turbinate facilitated heat and moisture exchange of inspired air [20].

In a departure from previous surgical models in which a laminar flow assumption was made [9,19], a turbulent flow was implemented in the computational fluid mechanics software using κ - ω model with the shear stress transport (SST). For low flow rates such as that simulated in this study, there is no significant difference in the airflow characteristics between the laminar and turbulent models. In fact, small local vortices may be better identified using a turbulent model. The use of κ - ω model with the SST option ensures that the simulations behave appropriately in both the near-wall (more prone to be turbulent) and far-field regions (more laminar). Generally, the existence of turbulence changes local flow patterns greatly and helps to enhance local heat and mass transfer. Simulating turbulent flow required greater computational processing than laminar flow modelling, and remains a challenging and controversial problem [21-,23]. The laminar, transition and turbulence regions are not well understood in the complex nasal cavity, especially for noses with different nasal physiological symptoms. For the current nasal models with inferior turbinate resection, turbinate reduction increases airway struc-

ture complexity, increases abrupt change in local flow velocity and may induce local turbulence more easily.

It is acknowledged that the virtual surgical procedures simulated on the current models may not represent true life situations. In a clinical situation, enlargement of the inferior turbinate may not be in a circumferential manner throughout the entire structure as simulated in this study. However, the current results provide a basis for future studies to use the hypertrophic turbinate model to evaluate surgical outcomes using CFD simulation. The results of this study do not necessarily endorse partial or total turbinate resection as the preferred surgical technique but it is obvious that radical surgery result in significantly adverse flow dynamics. The current preferred surgical method of turbinoplasty, described by Joniau et al. [24], is difficult to simulate. However, the surgical outcome of turbinoplasty resulted in the reduction of the inferior turbinate, which appeared similar to our current model of resecting the lower one-third. Thus, we believe the results can also be extrapolated for turbinoplasty. Other tissue volume reduction methods such as radiofrequency, Coblation® and laser may result in different aerodynamic but it is conceivably more difficult to simulate these techniques than gross reduction of the turbinate. Indeed, comparing simulations using pre- and post-surgery MRI scans would also be required to fully appreciate the effects of turbinate reduction surgery on nasal aerodynamics.

CONCLUSION

This study demonstrated that the nasal flow patterns for inferior turbinate hypertrophy and following turbinate surgery were significantly different from that of a healthy nasal cavity. The existence of vortices induced by turbinate pathology and surgical intervention increases local velocity, shear stress, and total pressure drop values. The implication of these changes is that the surgical procedures may need to be carefully planned to minimize impact on the normal functions of the nose. Using CFD techniques, it is now possible to evaluate the effects of inferior turbinate reduction surgery on nasal aerodynamics. It appears that conservative turbinate surgery results in near normal intra-nasal aerodynamics although further studies using real patients are required. The results were based on a single individual and cannot be generalised without similar studies in other subjects.

ACKNOWLEDGEMENT

The authors would like to acknowledge the financial support of the Academic Research Grant (T208A3103) from the Ministry of Education, Singapore. The work done under the project has been approved by the relevant Institutional Review Board. Dr Samuel C. Leong is the Rhinology Journal Traveling Fellow 2009/10.

REFERENCES

1. Batra PS, Seiden AM, Smith TL. Surgical management of adult inferior turbinate hypertrophy: a Systematic Review of the Evidence. Laryngoscope 2009; 119: 1819-1827.
2. Davis SS, Eccles R. Nasal congestion: mechanisms, measurement and medications. Core information for the clinician. Clin Otolaryngol Allied Sci 2004; 29: 659-666.
3. Leong SC, Chen XB, Lee HP, Wang DY. A review of the implications of computational fluid dynamic studies on nasal airflow and physiology. Rhinology 2010; 48: 139-145.
4. Chen XB, Lee HP, Hin Chong VF, Wang DY. Assessment of septal deviation effects on nasal air flow: A computational fluid dynamics model. Laryngoscope 2009; 119: 1730-1736.
5. Pless D, Keck T, Wiesmiller KM, et al. Numerical simulation of airflow patterns and air temperature distribution during inspiration in a nose model with septal perforation. Am J Rhinol 2004; 18: 357-362.
6. Grant O, Bailie N, Watterson J, et al. Numerical model of a nasal septal perforation. Stud Health Technol Inform 2004; 107: 1352-1356.
7. Lindemann J, Brambs HJ, Keck T, et al. Numerical simulation of intranasal airflow after radical sinus surgery. Am J Otolaryngol 2005; 26: 175-180.
8. Lindemann J, Keck T, Wiesmiller KM, et al. Numerical simulation of intranasal air flow and temperature after resection of the turbinates. Rhinology 2005; 43: 24-28.
9. Wexler D, Segal R, Kimbell J. Aerodynamic effects of inferior turbinate reduction- computational fluid dynamics simulations. Arch Otolaryngol – Head and Neck Surg 2005; 131: 1102-1107.
10. Lee HP, Poh HJ, Chong FH, et al. Changes of airflow pattern in inferior turbinate hypertrophy: a computational fluid dynamics model. Am J Rhinol Allergy 2009; 23: 153-158.
11. Liu Y, Edgar AM, Gu JJ, et al. Numerical simulation of aerosol deposition in a 3-D human nasal cavity using RANS, RANS/EIM, and LES. J Aerosol Sci. 2007; 38: 680-700.
12. Xi JX, Longest PW, Numerical predictions of submicrometer aerosol deposition in the nasal cavity using a novel drift flux approach. Int J Heat Mass Transf. 2008; 51: 5562-5577.
13. Hooper RG, Forced Inspiratory Nasal Flow–volume Curves, A Simple Test of Nasal Airflow. Mayo Clin Proc. 2001, Proc., 76: 990-994.
14. Guilherme Garcia JM, Neil B, Martins DA, et al. Atrophic rhinitis: a CFD study of air conditioning in the nasal cavity. J Appl Physiol 2007; 103: 1082-1092.
15. Moore EJ, Kern EB. Atrophic rhinitis: a review of 242 cases. Am J Rhinol 2001; 15: 355-361.
16. Naftali S, Rosenfeld M, Wolf M, et al. The air-conditioning capacity of the human nose. Ann Biomed Eng. 2005; 33: 545-53.
17. Grützenmacher S, Lang C, Mlynski G. The combination of acoustic rhinometry, rhinoresistometry and flow simulation in noses before and after turbinate surgery: a model study. ORL J Otorhinolaryngol Relat Spec. 2003; 65: 341-347.
18. Grützenmacher S, Robinson DM, Grafe K, et al. First findings concerning airflow in noses with septal deviation and compensatory turbinate hypertrophy - a model study. ORL J Otorhinolaryngol Relat Spec. 2006; 68: 199-205.
19. Hörschler I, Brücker Ch, Schröder W, et al. Investigation of the impact of the geometry on the nose flow. Eu J Mechanics B/Fluids 2006; 25: 471-490.
20. Schroter RC, Watkins NV. Respiratory heat exchange in mammals. Respir Physiol. 1989; 78: 357-369.
21. Liu Y, Edgar AM, Gu JJ, et al. Numerical simulation of aerosol deposition in a 3-D human nasal cavity using RANS, RANS/EIM, and LES. J Aerosol Sci 2007; 38: 683-700.
22. Xi JX, and Longest PW. Numerical predictions of submicrometer aerosol deposition in the nasal cavity using a novel drift flux approach. Int J Heat Mass Transf. 2008; 51: 5562-5577.

23. Inthavong K, Tian ZF, Li HF, et al. A numerical study of spray particle deposition in a human nasal cavity. Aerosol Sci Technol. 2006; 40:1034-1045.
24. Joniau S, Wong I, Rajapaksa S, Carney SA, Wormald PJ. Long-term comparison between submucosal cauterization and powered reduction of the inferior turbinates. Laryngoscope; 2006;116 (9): 1612-1616.

Assoc Prof. De Yun Wang, MD, PhD
Department of Otolaryngology
Yong Loo Lin School of Medicine
National University of Singapore
5 Lower Kent Ridge Road
Singapore 119260

Tel: +65-677 25373
Fax: +65-677 53820
E-mail: entwdy@nus.edu.sg

ORIGINAL CONTRIBUTION

Rhinology, 48, 401-407, 2010

Dexamethasone-induced apoptosis of freshly isolated human nasal epithelial cells concomitant with abrogation of IL-8 production*

S. Bobic[1], C.M. van Drunen[2], I. Callebaut[1], V. Hox[1], M. Jorissen[3], W.J. Fokkens[2], P.W. Hellings[1,3]

[1] Laboratory of Experimental Immunology, Catholic University Hospitals, Leuven, Belgium
[2] Department of Otorhinolaryngology, Academic Medical Center, Amsterdam, the Netherlands
[3] Department of Otorhinolaryngology, Head and Neck Surgery, Catholic University Hospitals, Leuven, Belgium

SUMMARY

Background: *Human nasal epithelial cells (hNECs) are the first line of immune defense and are able to produce mediators that recruit, activate and prolong survival of immune cells, among which IL-8 takes an important place. This study investigates the contribution of freshly isolated hNECs to IL-8 production in chronic rhinosinusitis with nasal polyps (CRSwithNP). Secondly, the effects of dexamethasone treatment on hNEC apoptosis and IL-8 production are investigated.*

Methodology: *hNECs were isolated from nasal polyps and healthy inferior turbinate of NP patients and from inferior turbinates of healthy donors by protease treatment and two negative selection procedures. hNECs were incubated with IL-1β, TNF-α or dexamethasone. After 24h, IL-8 levels were determined in the supernatants by ELISA. Finally, hNECs were incubated with increasing doses of dexamethasone and apoptosis was studied.*

Results: *hNECs isolated from nasal turbinates of healthy and NP patients and polyp tissue from NP patients produced similar levels of IL-8. IL-1β induced higher levels of IL-8 production in all types of hNECs without differences between control and NP tissue. Dexamethasone induced apoptosis of hNECs concomitant with abrogation of IL-8 production by hNECs.*

Conclusions: *IL-8 production by human nasal epithelial cells does not differ between NP and healthy tissue under baseline nor stimulatory conditions. Dexamethasone induces apoptosis of hNECs and abrogates IL-8 production.*

Key words: IL-8, human nasal epithelial cells (hNECs), chronic rhinosinusitis with nasal polyps (CRSwithNP) and dexamethasone

INTRODUCTION

Epithelial cells lining the nasal cavity have a pivotal role in detecting and responding to various environmental stimuli. Nasal epithelial cells are more than just a physical barrier. They exert their immunological function by producing various cytokines and growth factors that enable the recruitment and effector function of immune cells [(1)]. In addition, supernatants from cultured nasal or airway epithelial cells have been shown to prolong the survival of neutrophils [(2)] and eosinophils [(3)]. Many authors have studied airway epithelial cell biology using either immortalized cell lines [(1,4-6)] or freshly isolated nasal/airway epithelial cells. In most studies, primary epithelial cells obtained by positive selection are grown for 6-14 days in a medium rich in growth factors and mediators that stimulate growth of epithelial cells and apoptosis of other cell types [(2,6-9)]. Although these techniques yield 99,5% pure epithelial cell cultures, long term incubation might introduce immunological alterations in parallel with variations in phenotypical aspects of epithelial cells [(10-12)]. Here we build further on a recently reported novel technique of isolation and purification of primary nasal epithelial cells (hNECs) using two negative selections [(13)]. Epithelial cells were freshly isolated and incubated to study the contribution of human nasal epithelial cells (hNECs) to IL-8 production in chronic rhinosinusitis with nasal polyps (CRSwithNP).

IL-8 is one of the major cytokines secreted by epithelial cells upon stimulation. It is mainly produced upon stimulation of the toll-like receptors (TLRs) on the surface of the epithelial cells by an antigen [(14)] or microbial products. Super-antigens *Staphylococcus aureus* enterotoxin A (SEA) and B (SEB) [(15)]

*Received for publication: February 3, 2010; accepted: April 12, 2010

DOI:10.4193/Rhino10.033

and pro-inflammatory cytokines such as IL-1β [5,16], TNF-α [8,16] and IL-17 [17,18] can induce or modulate IL-8 production by human epithelial cells. Endothelin-1 [19] and VIP [20] were also shown to be potent inducers of IL-8 in human nasal epithelial cells. IL-8 acts through the G protein-coupled serpentine receptors CXCR1 and CXCR2 and its primary function is the recruitment of neutrophils to the site of inflammation. It is also known as neutrophil-chemotactic factor or CXCL8 [21].

CRSwithNP is characterised by a Th2 type inflammation associated with high levels of IL-8 and neutrophils in NP tissue [22]. It has been shown that IL-8 is up-regulated in CRS patients with NP being mainly produced by epithelial cells and eosinophils [23,24]. IL-8 is the major chemo-attractant factor for neutrophils, but the precise contribution of neutrophil influx in NP disease remains obscure. By releasing TGF-β [25] and matrix metalloproteinase 9 [26], neutrophils contribute to the reorganization of the extracellular matrix and the pathology of NP disease.

In this study, we aimed to investigate the effect of dexamethasone on nasal epithelial cell survival and IL-8 production. Dexamethasone represents a corticosteroid with broad anti-inflammatory potential. The use of corticosteroids in the treatment of NP disease is wide-spread as it is the only currently available treatment option with proven efficacy in NP [27]. Dorscheid et al. described dexamethasone-induced apoptosis of airway epithelial cells, in both primary and immortalized cell lines [6]. In addition, it has been shown that dexamethasone reduces the levels of IL-8 in human airway epithelial cells by different mechanisms: up-regulating glucocorticoid-induced leucine zipper (GILZ) which inhibits the transcription of NF-κB [28], by inhibiting the binding of NF-κB transcription factor to its responsive elements [29] or by destabilizing the IL-8 mRNA transcript [30]. In addition, bacterial products such as LPS and peptidoglycans increase the activity NF-κB in paranasal sinus epithelial cells which is suppressed by pre-incubation with dexamethasone [31]. However, there are reports of corticosteroid treatment inducing higher production of IL-8 in airway epithelial cells of asthmatic patients together with neutrophilic airway inflammation being associated with unresponsiveness to corticosteroid therapy [32].

Table 1. Patients' characteristics.

	Control patients (n = 19)	NP patients (n = 12)
Females	7/19 (37%)	6/12 (50%)
Nasal corticosteroids	7/19 (37%)	10/12 (83%)
Atopy	7/19 (37%)	6/12 (50%)
Asthma	1/19 (5%)	5/12 (42%)
AIA	0/19 (0%)	2/12 (17%)
Current smokers	4/19 (21%)	3/12 (25%)

* Patients are characterized by the presence of atopy, asthma (or AIA – aspirin-induced asthma syndrome), smoking habits and usage of nasal corticosteroids.

METHODS

Patients' characteristics

Nasal biopsies were taken from patients during surgery, after a written informed consent was obtained. A biopsy of the inferior turbinate and a piece of nasal polyp tissue were taken during surgery from CRS patients with nasal polyps (CRSwithNP, n = 12), while a biopsy of the inferior turbinate was obtained from healthy control patients (n = 19) without endoscopic evidence of CRSwithNP who underwent surgery for anatomical or aesthetical reasons. Patients' characteristics are listed in Table 1. The diagnosis of atopy was based on positive skin prick test results for a panel of 18 common inhalant allergens (HAL Allergy, Leiden, The Netherlands). The diagnosis of aspirin-intolerance and asthma were history based. The study was approved by the ethical committee of the Catholic University Hospital Leuven.

Isolation and stimulation of nasal epithelial cells (NECs)

A highly purified epithelial cell population was obtained by the following procedure (Figure 1) as reported previously [13]. Tissue was washed in sterile saline and enzymatically digested in 0.1% pronase (Protease XIV, Sigma) solution in culture medium (Lonza BioWhittaker DMEM) supplemented with L-Glutamine, 100 U/ml penicillin, 100 □g/ml streptomycin, and 2% (v/v) ultroser G. After overnight incubation at 4°C with shaking, the protease reaction was stopped by the addition of FCS (1:10 (v/v)). Cells were washed in culture medium and pelleted by centrifugation for 5 min on 800 rpm. Washed cells were re-suspended in 10 ml culture medium and incubated in a plastic culture flask for 1 h at 37°C in a cell incubator to remove the fibroblasts. The cell suspension was mixed with 2 x 10^7 prewashed CD45-magnetic beads (Dynabeads® CD45, Invitrogen) and epithelial cells were purified by the negative selection following the manufacturer's instructions (Figure 1). Cell purity was verified by cytospin preparations and was found to be ≥ 98%. The final cell suspension was centrifuged and re-suspended in 1 ml culture medium.

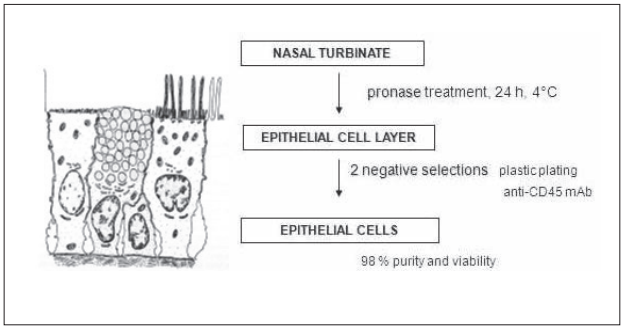

Figure 1. Purification procedure of human nasal epithelial cells (hNECs).